Numerical investigation of inelastic Fluid Flows based on Artificial Compressibility Method

Ruqaya S. Zwainy[1*], and *Anas Al-Haboobi*[1]

[1]Department of Mathematics, Faculty of Computer Sciences & Mathematics, University of Kufa, Kufa, Iraq.

Abstract. This article presents a numerical investigation of two distinct incompressible non-Newtonian flow configurations. The first one deals with flow through a straight channel, the second one concerns flow in a square cavity subjected to the uniform translation of the upper lid at a given velocity both in two-dimensional space. For both geometries, analytical solutions are derived and subsequently employed to define appropriate boundary conditions. Numerically, the governing equations is solved by an artificial compressibility approach in combination with the Galerkin finite element method. Fluid system is governed by the Navier-Stokes equations (N-S), and non-Newtonian characteristics are captured using the power-law constitutive relation. The work systematically investigates the influence of changes in power-law index (n) on velocity and pressure fields for both flows. Moreover, convergence characteristics of the numerical scheme being considered are discussed and for all tested n -values an efficient and reliable convergence within a velocity field is observed. The presented data is validated against the state-of-art data available in the literature leading to concurrence with existing results thus ensuring strength and robustness of the methodology.

Keywords: Artificial Compressibility, Inelastic flow, Lid-Driven cavity, non-Newtonian flow, Power-law model.

1 Introduction

Numerical solutions of the two-dimensional N-S equations have gained significant interest in computational fluid dynamics (CFD) over the past few decades due to their wide applicability to physical and engineering applications. The N-S equations are at the heart of modelling a variety of both Newtonian and non-Newtonian fluid flows in many engineering systems.

Mathematically however, these equations have an analytical solution only for a small number of idealized conditions, despite the fact that in practice many flow situations are described by these equations. This increasing complexity in physical models, the properties

[*] Corresponding author: ruqayas.zwainy@student.uokufa.edu.iq

of materials, and boundary conditions has made numerical methods become more or less employed as the only means of solving governing equations.

Especially in the fields of numerical science and engineering, incompressible non-Newtonian fluid flow over canonical geometries (straight channels, and lid-driven cavities) has attracted long lasting interest among researchers forming part of the fluid dynamics community. These flows respect conservation of mass as well as time-dependent momentum, described here in Cartesian coordinates at isothermal conditions (see Bird et al. [1] for details). Even though the geometries of straight channel and square lid driven cavity are basic, they represent fundamental benchmark problems and are important to fluid mechanic research and industrial applications. In this study, Poiseuille flow in a two-dimensional straight channel under isothermal conditions is first examined, followed by the classical square lid-driven cavity flow problem. Numerous studies have investigated incompressible Newtonian and non-Newtonian flows using a variety of numerical techniques for both straight-channel flows [2-6] and lid-driven cavity flows [7-11].

In this paper, a comprehensive numerical investigation is presented for an incompressible, inelastic power-law fluid, whose apparent viscosity depends on the local shear rate. The artificial compressibility method (ACM) is coupled with the Galerkin finite element formulation and applied to the Navier-Stokes equations expressed in Cartesian coordinates for both the straight-channel and lid-driven cavity configurations. The ACM was modified the continuity equation of this elliptic incompressible system into a hyperbolic compressible one via an artificial time derivative of pressure. By this transformation the standard time-dependent solution procedures can be used, leading to convergence of a different order than that offered by conventional primitive variable formulations, which must solve another set of pressure correction equations at every time step. The artificial compressibility term goes to zero when the steady-state solution is reached. Computational results are presented for an inelastic, power-law non-Newtonian fluid within a lid-driven cavity configuration and represent the first implementation of the AC-FEM framework to this problem; insights into the coupling between shear-dependent viscosity effects and confinement-induced flow dynamics are shared. The study systematically examines the influence of n on the fundamental flow characteristics, including the velocity and pressure fields. Moreover, complete analytical solutions for both flow cases are derived and used to define boundary conditions. The numerically results are verified by comparison with the available benchmark solutions in the literature, indicating a very good agreement and verifying that the proposed AC--FEM is accurate, reliable and computationally effective. These results demonstrated the accuracy of the current model for simulating incompressible non-Newtonian flow in commonly used geometries.

2 Governing Equation

The non-dimensional incompressible non--Newtonian flow are expressed as [2, 3]:

$$\frac{\partial \mathrm{u}}{\partial x}+\frac{\partial \mathrm{v}}{\partial y}=0, \tag{1}$$

$x-$direction

$$\mathrm{Re}\left(\frac{\partial \mathrm{u}}{\partial t}+\mathrm{u}\frac{\partial \mathrm{u}}{\partial x}+\mathrm{v}\frac{\partial \mathrm{u}}{\partial y}\right)=-\frac{\partial p}{\partial x}+\eta\left(\frac{\partial^2 \mathrm{u}}{\partial x^2}+\frac{\partial^2 \mathrm{u}}{\partial y^2}\right), \tag{2}$$

$y-$direction

$$\mathrm{Re}\left(\frac{\partial \mathrm{v}}{\partial t}+\mathrm{u}\frac{\partial \mathrm{v}}{\partial x}+\mathrm{v}\frac{\partial \mathrm{v}}{\partial y}\right)=-\frac{\partial p}{\partial y}+\eta\left(\frac{\partial^2 \mathrm{v}}{\partial x^2}+\frac{\partial^2 \mathrm{v}}{\partial y^2}\right). \tag{3}$$

Where η, u, v, and p are the dynamic viscosity, velocity components, and pressure, respectively.

Here, (Re) is Reynolds number that is defined as [3] :

$$\mathrm{Re} = \frac{\rho_\infty U_\infty L}{\eta_\infty}.$$

Since the fluid under consideration exhibits non-Newtonian behavior, its viscosity is no longer fixed but varies with the applied shear rate. Accordingly, the dynamic viscosity is evaluated using the power-law model, defined as [4]:

$$\eta = k(\dot{\gamma})^{n-1} = k(\sqrt{2(\frac{\partial \mathrm{u}}{\partial x})^2 + (\frac{\partial \mathrm{v}}{\partial x} + \frac{\partial \mathrm{u}}{\partial y})^2 + 2(\frac{\partial \mathrm{v}}{\partial y})^2})^{n-1}. \quad (4)$$

Where, $\dot{\gamma}$ denotes the shear rate, k is the consistency coefficient, and n is the power-law index characterizing the degree of shear-thinning ($n < 1$) or shear-thickening ($n > 1$) behavior of the fluid.

3 Numerical Method

We will use the ACM to solve the system of non-Newtonian governing equations. The essential idea of the ACM is to transform the elliptic incompressible system into a mixed hyperbolic parabolic form by adding AC-term to the continuity equation. This artificial term introduces a pseudo time derivative of pressure, thereby enabling the use of standard time-dependent solution techniques. Importantly, the AC-term vanishes as the steady-state solution is reached, ensuring that the original incompressibility condition is satisfied. To demonstrate the use of this strategy, the term artificial compressibility was added to the continuity equation. Consequently, Eq. (1), is modified and expressed as:

$$\frac{\partial \rho}{\partial t} + \frac{\partial \mathrm{u}}{\partial x} + \frac{\partial \mathrm{v}}{\partial y} = 0. \quad (5)$$

Where, ρ denotes the artificial density, which is introduced solely for numerical purposes. This artificial density is related to the pressure through a prescribed artificial equation of state as:

$$\frac{\partial \rho}{\partial t} = \frac{1}{B_{\mathrm{ac}}} \frac{\partial p}{\partial t}. \quad (6)$$

Here, B_{ac} denotes the artificial compressibility parameter, where $0 < \frac{1}{B_{\mathrm{ac}}} \ll 1$. By substituting Eq. (6) into Eq. (5), the continuity equation is reformulated into its artificial compressibility form, referred to as the artificial compressibility continuity equation, expressed as:

$$\frac{1}{B_{\mathrm{ac}}} \frac{\partial p}{\partial t} + \frac{\partial \mathrm{u}}{\partial x} + \frac{\partial \mathrm{v}}{\partial y} = 0. \quad (7)$$

Using the Galerkin-FEM to the system of Eqs. (2), (3) and (7). Now, to convert the systems to matrices formulations, the velocity and pressure will be approximated by used of shape functions as follows:

$$\mathrm{u} = \sum_{i=1}^{\overline{n}} \psi_i(x,y)\mathrm{u}_i(t),\ \mathrm{v} = \sum_{i=1}^{n} \psi_i(x,y)\mathrm{v}_i(t),\ p = \sum_{j=1}^{\overline{m}} \Phi_j(x,y)p_j(t). \quad (8)$$

the symbol $\overline{m}$ represents the number of vertices of triangular elements, while $\overline{n}$ denotes the total number of nodes in the computational the mesh. The vector values at nodes for both velocity and pressure are defined by $\mathrm{u}_i(t)$, $\mathrm{v}_i(t)$ and $p_j(t)$, respectively. $\psi_i(x,y)$ and

$\Phi_j(x,y)$ are quadratic and linear shape functions used to represent the distribution of velocity and pressure among nodes within the computational domain. These functions are utilized to create approximated continuous fields and conduct integrative processes in the construction of FEM equation.

By applying the divergence theorem and subsequently rearranging terms, the weak form of the two-dimensional N-S equations, is obtained as:

$$\left[M_p\right][\dot{p}] + \left[Q_1^T\right][\mathrm{u}] + \left[Q_2^T\right][\mathrm{v}] = 0, \tag{9}$$

$$[M][\dot{\mathrm{u}}] + [C(\mathrm{u},\mathrm{v})][\mathrm{u}] - \frac{1}{\mathrm{Re}}[Q_1][p] + \frac{\eta}{\mathrm{Re}}[K_{11}][\mathrm{u}] + \frac{\eta}{\mathrm{Re}}[K_{22}][\mathrm{u}] = 0, \tag{10}$$

$$[M][\dot{\mathrm{v}}] + [C(\mathrm{u},\mathrm{v})][\mathrm{v}] - \frac{1}{\mathrm{Re}}[Q_2][p] + \frac{\eta}{\mathrm{Re}}[K_{11}][\mathrm{v}] + \frac{\eta}{\mathrm{Re}}[K_{22}][\mathrm{v}] = 0. \tag{11}$$

Such that,

$$[M] = \int_{\Omega^e} \curlyvee \curlyvee^T d\Omega,\ \left[M_p\right] = \int_{\Omega^e} \Phi\Phi^T d\Omega$$

$$[C(\mathrm{u})] = \int_{\Omega^e} \left(\curlyvee \curlyvee^T \mathrm{u}\frac{\partial \curlyvee^T}{\partial x}\right) d\Omega,\ [C(\mathrm{v})] = \int_{\Omega^e} (\curlyvee \curlyvee^T \mathrm{v}\frac{\partial \curlyvee^T}{\partial y}) d\Omega$$

$$[K_{11}] = \int_{\Omega^e} \left(\frac{\partial \curlyvee}{\partial x}\frac{\partial \curlyvee^T}{\partial x}\right) d\Omega,\ [K_{22}] = \int_{\Omega^e} (\frac{\partial \curlyvee}{\partial y}\frac{\partial \curlyvee^T}{\partial y}) d\Omega$$

$$[Q_1] = \int_{\Omega^e} \frac{\partial \curlyvee}{\partial x}\Phi^T d\Omega,\ [Q_2] = \int_{\Omega^e} \frac{\partial \curlyvee}{\partial y}\Phi^T d\Omega$$

Finally, the matrices formula above can be rewrite in the system of matrix formulations as:

$$\begin{bmatrix} M & 0 & 0 \\ 0 & M & 0 \\ 0 & 0 & M_p \end{bmatrix}\begin{bmatrix} \dot{\mathrm{u}} \\ \dot{\mathrm{v}} \\ \dot{p} \end{bmatrix} + \begin{bmatrix} S & 0 & -\frac{1}{\mathrm{Re}}Q_1 \\ 0 & S & -\frac{1}{\mathrm{Re}}Q_2 \\ Q_1^T & Q_2^T & 0 \end{bmatrix}\begin{bmatrix} \mathrm{u} \\ \mathrm{v} \\ p \end{bmatrix} = \begin{bmatrix} 0 \\ 0 \\ 0 \end{bmatrix}, \tag{12}$$

such that

$$[S] = [C(\mathrm{u})] + [C(\mathrm{v})] + \frac{\eta}{\mathrm{Re}}[K_{11}] + \frac{\eta}{\mathrm{Re}}[K_{22}].$$

To handle the nonlinear terms in the system of Eq. (12), the Newton–Raphson iterative method is employed. The implementation details of the algorithm have been described in Figure 1.

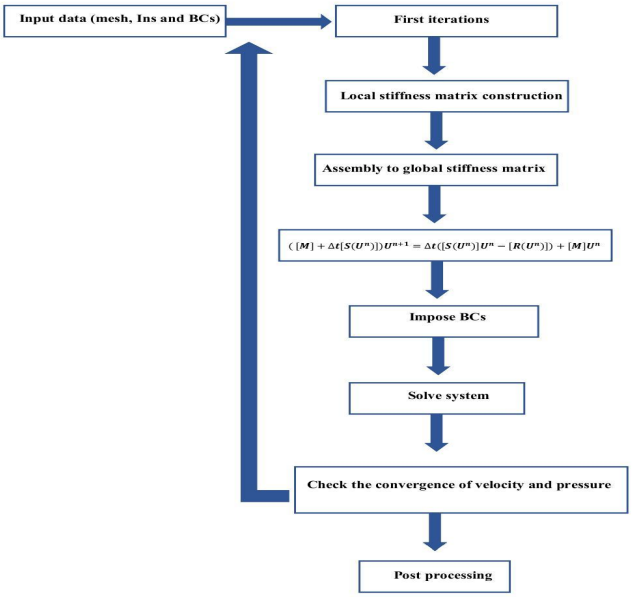

Fig. 1. Algorithm of AC-FEM.

4 Exact Solutions under specific conditions

4.1 Rectangular Channel

Finding exact solutions of Navier--Stokes equations display mathematical difficulties because of the nonlinear terms of equations. However, there is a special solution area for incompressible non-Newtonian isothermal flow, for which the continuity equation and momentum equation are expressed as:
Continuity

$$\frac{\partial \mathrm{u}}{\partial x}+\frac{\partial \mathrm{v}}{\partial y}=0, \tag{13}$$

Momentum

$$\rho\left(\frac{\partial \mathrm{u}}{\partial t}+\mathrm{u}\frac{\partial \mathrm{u}}{\partial x}+\mathrm{v}\frac{\partial \mathrm{u}}{\partial y}\right)=-\frac{\partial p}{\partial x}+\eta\left(\frac{\partial^2 \mathrm{u}}{\partial x^2}+\frac{\partial^2 \mathrm{u}}{\partial y^2}\right), \tag{14}$$

In the case of the axisymmetric flow with vanishing tangential and radial velocities $\frac{\partial \mathrm{u}}{\partial x}=\frac{\partial^2 \mathrm{u}}{\partial x^2}=0$ and $\frac{\partial \mathrm{u}}{\partial t}=0, \mathrm{v}=0$. Thus Eqs. (13) and (14) will be reduce as:

$$0=-\frac{\partial p}{\partial x}+\eta+\frac{\partial^2 \mathrm{u}}{\partial y^2}. \tag{15}$$

By integrating Eq. (15), we have:

$$u=\frac{1}{\eta}\left(\frac{\partial p}{\partial x}\frac{y^2}{2}+c_1 y+c_2\right).$$

By imposing the boundary conditions, at $y = \pm h$ for $\mathrm{u} = 0$, we have the general solution as:

$$\mathrm{u} = \frac{1}{2\eta}\frac{\partial p}{\partial x}(y^2 - h^2). \tag{16}$$

By substitute maximum velocity into Eq. (16) we get:

$$\mathrm{u}_{\max} = \frac{1}{2\eta}\frac{\partial p}{\partial x}(-h^2). \tag{17}$$

Thus, the analytic solution defined as:

$$\begin{aligned} u_{\text{exact}} &= \frac{\mathrm{u}}{\mathrm{u}_{\max}}, \\ &= 1 - \frac{y^2}{h^2}. \end{aligned} \tag{18}$$

4.2 Square Lid-driven Cavity

Let

$$\boldsymbol{S} = \frac{\mathbf{x}}{\boldsymbol{L}}. \tag{19}$$

Here, **S** is a dimensional variable, **L** represents the characteristic length.

$$\boldsymbol{F(S) = G\mathbf{u}_{\max}(S)^2(1-S)^2}. \tag{20}$$

Substituting the given values $\boldsymbol{S} = \frac{\mathbf{1}}{\mathbf{2}}$, into the Eq. (20), gives us the following result:

$$\begin{aligned} \boldsymbol{F\left(\frac{1}{2}\right) = G\left(\frac{1}{2}\right)^2\left(1-\frac{1}{2}\right)^2}, \\ \boldsymbol{= G\left(\frac{1}{16}\right)}, \\ \boldsymbol{G = 16}. \end{aligned} \tag{21}$$

By substituting Eq. (19) and (21) into Eq. (20) gives

$$\mathbf{u(x) = 16u_{\max}\left(\frac{x}{L}\right)^2\left(1-\frac{x}{L}\right)^2}. \tag{22}$$

5 Problem Specification and Boundary Conditions

To validate the proposed algorithm, two benchmark problems representative of incompressible non-Newtonian flows are considered. The first benchmark involves fully

developed Poiseuille flow in a straight channel with two-dimensional axial geometry under isothermal conditions. The second benchmark is the classical square lid-driven cavity problem, in which the flow is induced by the uniform motion of the upper lid at a prescribed velocity.

For both test cases, a structured mesh composed of triangular finite elements is employed, as illustrated in Figure 2, while the characteristic parameters of a representative mesh are summarized in Table 1. The boundary conditions applied to the two benchmark problems are specified as follows (see Figure 3):

Channel problem:

1- Poiseuille flow (ps), Eq. (18) at the entrance is specified with zero radial velocity.
2- No-slip BCs is applied to the upper and lower walls of the channel.
3- For the channel outlet both pressure and radial velocity, be zero.

Lid driven cavity problem:

1- At the upper boundary, the tangential velocity with a variable profile which defined at Eq. (22) is applied to push the fluid flow in the cavity with a variable profile.
2- No-slip BCs are enforced on the remaining three stationary walls.

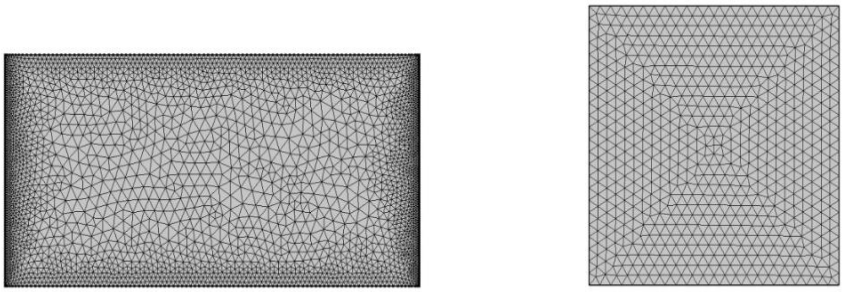

(a) Rectangular Channel (b) Square Lid-driven Cavity

Fig. 2. Structured finite element meshes.

Table 1. Type of generated meshes.

Geometry	Total Elements	Number of vertices	Degrees of freedom
Channel	5964	3183	9549
Driven Cavity	1308	701	2103

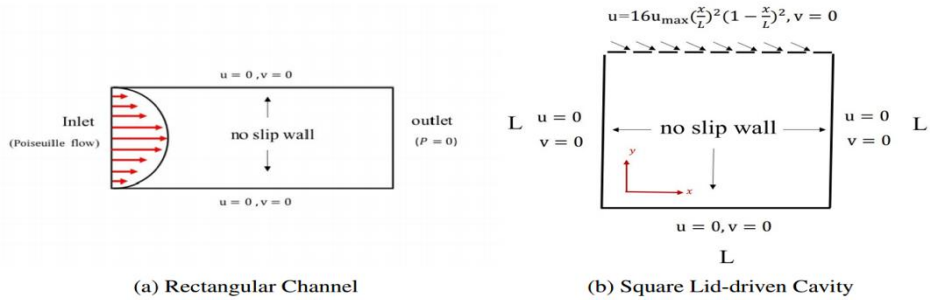

Fig. 3. The problem's geometry and boundary conditions.

6 Result and Discussion

In this study, two canonical numerical test cases, namely a two-dimensional straight channel and a lid-driven cavity, are considered to assess the performance and accuracy of the proposed algorithm. The numerical simulations focus on incompressible non-Newtonian flows, with particular emphasis on investigating influence of n on solution variables. The main results are directed to explaining effect of n on both velocity and pressure fields. All results that will be presented and discussed will be based on a constant artificial compression coefficient of $B_{ac} = 1000$. This is due to the relation with Mach number The key relationship is inversely proportional.
To this end, an artificial compressibility formulation is solved in conjunction with the Galerkin finite element method governing equations. Numerical results are all shown in a cartesian coordinate system.

6.1 Channel flow

The velocity contours and the velocity vector fields for Re $= 1$ and $B_{ac} = 1000$, are shown in Figures 4 and 5 at power-law indices of $n = 0.5$ and $n = 1.5$, respectively. For laminar channel flow, the maximum axial velocity is located along the centerline of channel as expected. Top reason for this large difference is peak velocity, u $\approx$ 1.0 in the shear-thinning case ($n = 0.5$) and can goes to around u $\approx$ 1.1 in the shear-thickening case ($n =$ 1.5). This acceleration with growing n follows from the rheology of shear-thickening fluids where effective viscosity distribution across the channel changes [4].
Moreover, the maximum pressure also significantly increases with the power-law index from $p = 11.4$ to $p = 30.8$. Although the inlet pressure is highest and gradually reduces in axial direction toward the outlet, as seen in Figure 6, evidencing classical pressure driven flow behavior.
We illustrate the effect of different $n = \{0.5, 1, 1.5\}$ on axial pressure distribution in Figure 7. As one can easily note, the quantitative value of pressure is rising significantly with increasing n due to the associated rise in apparent viscosity which arises from shear-thickening behavior [4].

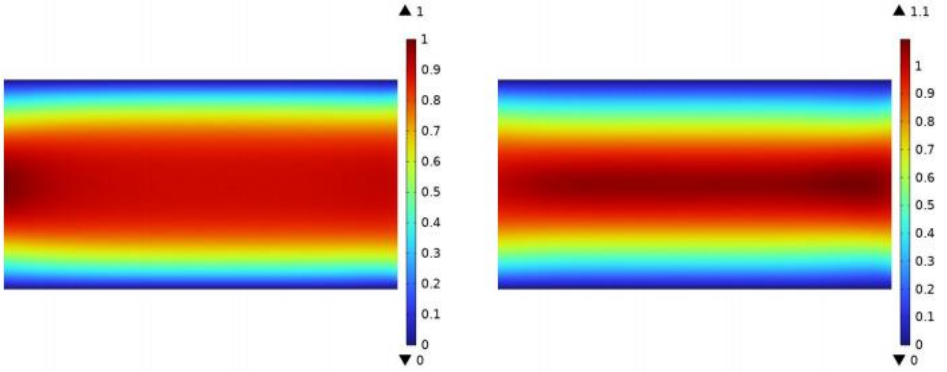

(a) $n = 0.5$ (b) $n = 1.5$

Fig. 4. Influence of n on velocity

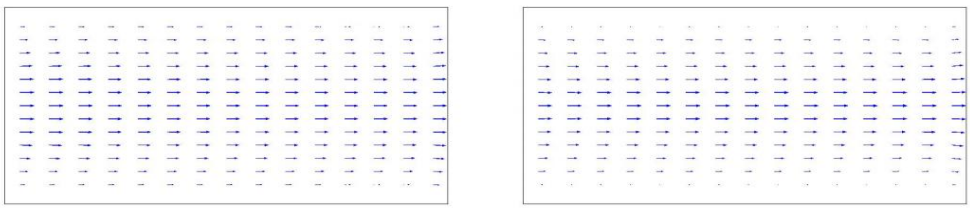

(a) $n = 0.5$ (b) $n = 1.5$

Fig. 5. Influence of n on velocity

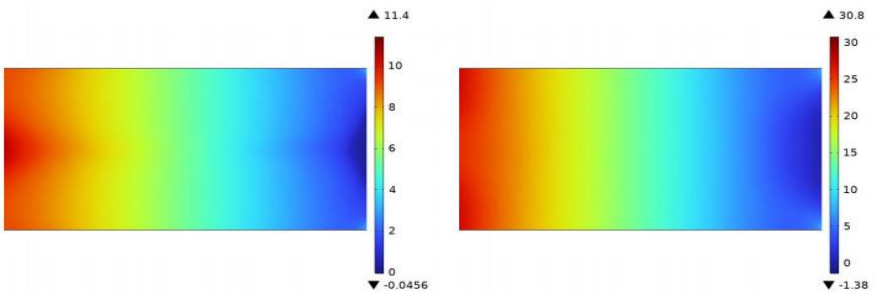

(a) $n = 0.5$ (b) $n = 1.5$

Fig. 6. Influence of n on pressure

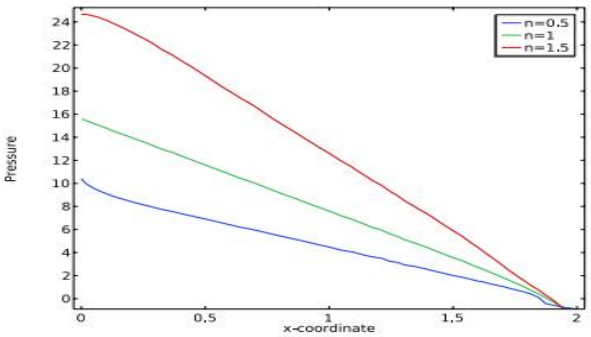

Fig. 7. Influence of n on pressure.

6.2 Driven cavity

This configuration is commonly used as a test case to study the accuracy and robustness of numerical schemes for incompressible flows [12]. Here, the flow is enclosed in a square cavity and motion occurs due to uniform movement of the top lid at a given velocity as defined by Eq. (22). Figures 8(a,b) show the axial velocity profiles for fixed Reynolds number $Re = 1$ and artificial compressibility parameter $B_{ac} = 1000$, for power-laws indices $n = 0.5$ and $n = 1.5$, respectively. In the region of moving lid, there is a clear gradient in velocity that can be ascribed to shear-thickening effects, that rally increases with index $n = 1.5$. Additionally, the stagnation zone is obviously identified in bottom left and bottom right of cavity region. Figures 8(c,d) show the pressure contours. Particularly, low-pressure regions develop both at the center of the primary vortex and near the upper left corner of the cavity; whereas a small stagnation point driven by horizontal velocity lies in close proximity to its upper right corner. The region is characterized by a pressure buildup that increases at higher power-law indices $n = 1.5$.

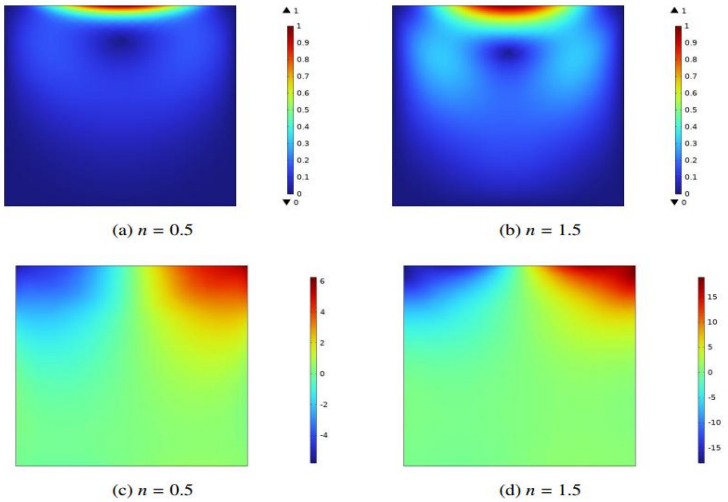

Fig. 8. Effect of n on both velocity and pressure.

In Figure 9 cavity velocity vector field is show. Top $U = 1$ wall, sign of moving lid effects the current is then directed along the right wall, cascades down it and rises again at the left one. For the shear-thickening case (n=1.5), this motion generates a strong central vortical structure that grows in extent and strength. All of these results were consistent with what was presented in [5,13].

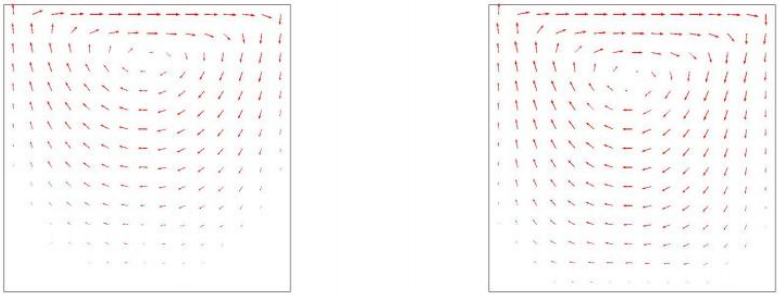

(a) $n = 0.5$ (b) $n = 1.5$

Fig. 9. Influence of n on velocity vector.

Fixed maintenance parameters $\mathrm{Re} = 1, k = 1$ and $B_{ac} = 1000$ are used to evaluate the effect of n where $n \in \{0.5, 1, 1.5\}$. The effect of n on the velocity profiles in the vertical and horizontal center lines of the cavity is shown in Figure 10. With decreasing size of n, the peak values of v-velocity decrease and vice versa for u-velocity. The shear-thinning character of the fluid plays a significant role here, as higher strain rates will have lower viscosity and thus encourage stronger horizontal flow whilst suppressing vertical velocity components, consistent with Neofytou's reports [14].

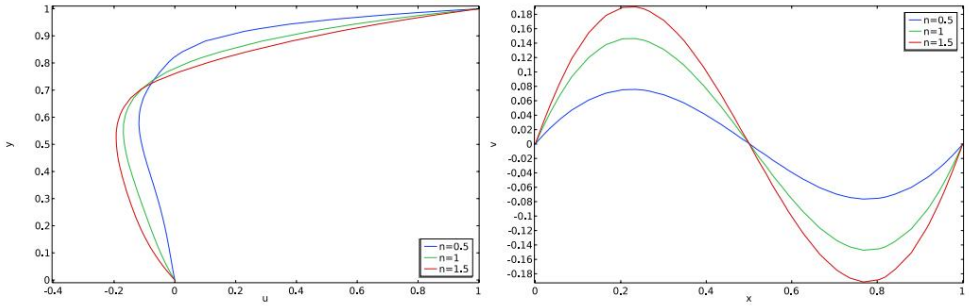

Fig. 10. Influence of n on velocity profiles along vertical .and horizontal centerline of cavity.

Figure 11 shows the convergence behavior of the error $\left||U|\right|_2$ of velocity for $n = \{0.5, 1, 1.5\}$. The results show consistently small errors which confirms the accuracy of the solutions computed and the stability of your numerical method. As can be seen in the above figure, the convergence rate is faster for Newtonian case $(n = 1)$ than it is for non-Newtonian cases.

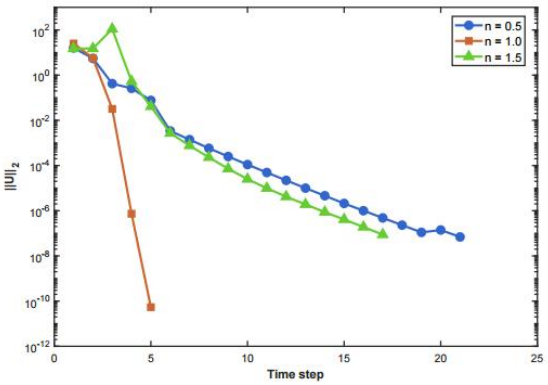

Fig. 11. Error convergence.

7 Conclusions

In this paper, two cases of representative incompressible non-Newtonian flow cases are numerically simulated. The former is referring to flow through a straight channel and the latter corresponds to flow confined in a square cavity forced by the motion of the upper lid. We have used an artificial compressibility method in conjunction with the Galerkin finite element technique to solve these equations. For both flow problems, a capture analysis of the velocity field is carried out for different values of n. In this context, the effectiveness of the proposed method is evaluated by systematically investigating the effect of n on both the velocity and pressure fields. Comparison of the shear thinning $(n = 0.5)$ and shear thickening $(n = 1.5)$ demonstrates that effects become more pronounced as power law index goes above unity consistent with characteristic properties of shear thickening fluids. In both geometry we conclude that when n increases then velocity and pressure for both geometries will increase too. The error convergence for different n value for velocity was included. The result shows a very good convergence rate especially for Newtonian case. The numerical values show good agreement with existing benchmark solutions and are in line with the typical physical features of the flow, confirming both the capability and efficiency of the proposed method. In our future work, we intend to study the same problem under non-isothermal conditions, which opens the door to exploring important applications in various engineering and industrial fields.

References

1. R. B. Bird, R. C. Armstrong, and O. Hassager, Dynamics of Polymeric Liquids, Vol. 1: Fluid Mechanics (John Wiley & Sons, New York, 1986).
2. A. Al-Haboobi and A. H. Al-Muslimawi, Simulation of Newtonian axisymmetric thermal channel flow by using a developed Taylor–Galerkin/Pressure Correction method. Int. J. Appl. Comput. Math. 11, **172** (2025). https://doi.org/10.1007/s40819-025-02010-9
3. A. Al-Haboobi and A. H. Al-Muslimawi, A new algorithm for solving thermal Newtonian flow in axisymmetric straight channel. Basrah J. Sci. **41**, 399–418 (2023). https://doi.org/10.29072/basjs.20230301

4. S. H. Al-Zaidi and A. Al-Haboobi, Investigation of inelastic power-law model under thermal conditions by using a developed method. Boletim da Sociedade Paranaense de Matemática **43**, 1–11 (2025). https://doi.org/10.5269/bspm.77563
5. J. R. Abdul-Jabbar, A. H. Al-Muslimawi, and I. A. Fadhel, Computational study of the flow of Newtonian fluid through a straight channel and lid-driven cavity. Iraqi J. Sci. **64**, 4043–4057 (2023). https://doi.org/10.24996/tjs.2023.64.8.28
6. I. A. Fadhel and A. H. Al-Muslimawi, Simulation of Oldroyd-B viscoelastic fluid in axisymmetric straight channel by using a hybrid finite element/volume method. J. Adv. Res. Fluid Mech. Therm. Sci. **81**, 26–40 (2021). https://doi.org/10.37934/arfmts.81.1.2640
7. S. Park, Direct numerical simulation for lid-driven cavity under various Reynolds numbers in fully staggered grid. Phys. Fluids **35**, 115110 (2023). https://doi.org/10.1063/5.0169148
8. J. Zhang, B. Xiao, and W. Yang, Numerical study of lid-driven square cavity flow with embedded circular obstacles using spectral/hp element methods. Appl. Sci. **12**, 11711 (2022). https://doi.org/10.3390/app122211711
9. N. Fatima, I. Rajan, D. A. Perumal, A. Sasithradevi, S. A. A. Ahmed, M. R. Gorji, and Z. Ahmad, Simulation of fluid flow in a lid-driven cavity with different wavelengths corrugated walls using lattice Boltzmann method. J. Taiwan Inst. Chem. Eng. **144**, 104748 (2023). https://doi.org/10.1016/j.jtice.2023.104748
10. M. R. Patel, J. U. Pandya, and V. K. Patel, Numerical analysis of fluid flow behaviour in porous media lid-driven cavity using the finite volume technique. Int. J. Appl. Comput. Math. 8, **153** (2022). https://doi.org/10.1007/s40819-022-01353-x
11. T. Vu-Huu, C. Le-Thanh, H. Nguyen-Xuan, and M. Abdel-Wahab, Polygonal finite element for two-dimensional lid-driven cavity flow. Comput. Mater. Contin. **70**, 4217–4239 (2022). https://doi.org/10.32604/cmc.2022.020889
12. U. Ghia, K. N. Ghia, and C. T. Shin, High-Re solutions for incompressible flow using the Navier–Stokes equations and a multigrid method. J. Comput. Phys. **48**, 387–411 (1982). https://doi.org/10.1016/0021-9991(82)90058-4
13. V. Hatic, B. Mavric, and B. Sarler, Meshless simulation of a lid-driven cavity problem with a non-Newtonian fluid. Eng. Anal. Bound. Elem. **131**, 86–99 (2021). https://doi.org/10.1016/j.enganabound.2021.06.015
14. P. Neofytou, A third-order upwind finite volume method for generalized Newtonian fluid
flows. Adv. Eng. Softw. **36**, 664–680 (2005).
https://doi.org/10.1016/j.advengsoft.2005.03.011